Small-scale auroral current sheet structuring

C. C. Chaston[1] and K. Seki[2]

[1]   We simulate the 3-D evolution of a thin current sheet as it impinges on the ionosphere from a magnetospheric source in a manner analogous to that which may occur during the onset of an auroral substorm. We consider two scenarios: one in which electron inertia alone acts to allow motion between the plasma and the geomagnetic field, and a second where a resistive layer at the interface between the ionosphere and magnetosphere is included. These two scenarios in our fluid model are intended to represent what have become known as "Alfvénic" and "Quasi-static" or "Inverted-V" aurora, respectively. In the absence of resistivity the evolution is shown to be driven by a combination of Kelvin-Helmholtz and tearing instabilities leading to vortices similar to folds and the eventual break-up of the planar arc into distorted fine-scale sheets and filamentary currents. The later stage of this evolution is driven by an instability on the steep transverse current gradients created by the former instabilities. With a resistive layer present the K-H instability dominates leading to the formation of auroral curls. We show how these evolutionary processes can be ordered based on the ratio of the transverse electric and magnetic fields ($\Delta E_X/\Delta B_Y$) across the current sheet relative to the Alfvén speed, and demonstrate how the evolution is dependent on wave reflection from the topside ionosphere.

1.   Introduction

[2]   The auroral substorm is a consequence of the explosive release of magnetic energy in the Earth's magnetotail [*Angelopoulos et al.*, 2008]. Observations exploiting optical imaging and low-altitude particle measurements along auroral flux tubes [*Mende et al.*, 2003] have demonstrated that the onset of a substorm occurs in a thin layer containing highly structured field-aligned currents carried by electrons having a mixture of flat-top and peaked spectra in differential energy flux as a function of energy. These features are the hallmark of acceleration processes in dispersive Alfvén waves [*Chaston et al.*, 1999] and quasi-static potential structures [*Evans*, 1974], respectively. When observed in isolation these features in electron energy-time spectrograms are often used to identify the "Alfvénic" and "Quasi-static" or "Inverted-V" aurora, respectively [*Paschmann et al.*, 2003].

[3]   Auroral forms observed at, and subsequent to, substorm onset exhibit a range of scales extending from structures with wavelength greater than 50 km [*Donovan et al.*, 2006]; down to multikilometer folds [*Hallinan and Davis*, 1970] and kilometer and subkilometer vortical (curls) and filamentary structures [*Trondsen and Cogger*, 1998]. On the largest scales the generation of these features are thought to

be due to the action of instabilities in the Earth's plasma sheet [*Roux et al.*, 1991], while on mesoscale and small scales the structuring is thought to occur through the action of instabilities along auroral field lines and in the ionosphere [*Hallinan and Davis*, 1970; *Seyler*, 1990; *Otto and Birk*, 1993; *Lysak*, 1991]. Significantly, the electron inertial length (λ_e) at altitudes above the topside ionosphere has a value of the order of 500 m to 10 km corresponding to the spatial range of small-scale folds and vortical auroral forms. *Seyler* [1990] and *Wu and Seyler* [2003] have demonstrated that the action of instabilities arising due to the effects of electron inertia such as tearing and instabilities on transverse current gradients in addition to shear-flow instabilities should play a role in the evolution of auroral current sheets on these scales.

[4]   Perhaps the simplest geometry appropriate for a consideration of auroral current sheet stability consists of an infinite planar geomagnetic field-aligned (B_o; Z) current sheet with half width "a" transverse (X) to B_o occupying a shear layer between equal but opposing flows $V_{1Y} = -V_{2Y}$. In this geometry the threshold velocity change for the Kelvin-Helmholtz (K-H) instability is approximately $\Delta V > 2V_{A\perp}$ [*Chandrasekar*, 1961] where $\Delta V = |V_{1Y}-V_{2Y}|$ is the magnitude of the velocity change and $V_{A\perp} = B_Y/(\mu_o\rho)^{1/2}$ is the Alfvén speed given by the transverse magnetic field (B_Y) outside the current sheet or shear layer. We note that the scale of the current sheet is implicitly included in this threshold through the magnitude of B_Y in $V_{A\perp}$. Taking $V_y = E_X/B_o$ the threshold can be written as $|E_X/B_Y| > V_A$ where E_X is the transverse electric field outside the shear layer. For current sheets which produce aurora the shear layer is

---

[1]Space Sciences Laboratory, University of California, Berkeley, California, USA.
[2]Solar Terrestrial Environment Laboratory, University of Nagoya, Nagoya, Japan.

also a negative charge layer [*Hallinan and Davis*, 1970]. Consequently, the threshold ΔV is generally larger due to ion shielding which can limit extent of V_{1Y} and V_{2Y} in X to widths comparable to the fastest growing wavelength [*Wagner et al.*, 1983]. For these more realistic geometries solution of the specific eigenvalue problem is required to determine the threshold [*Wu and Seyler*, 2003]. Nonetheless, the simple condition can be used to qualitatively define a maximum width of an auroral arc unstable to the K-H instability. For a field-aligned current density $J_\parallel$ the condition $\Delta V > 2V_{A\perp}$ requires

$$\Delta V > 2J_\parallel a \sqrt{\frac{\mu_o}{\rho}} \qquad (1)$$

where ρ is the plasma mass density and we have used Ampere's law to relate $J_\parallel$ and B_Y at the altitude where the instability occurs. In this expression $2J_\parallel a(\mu_o/\rho)^{1/2}$ is the minimum velocity change across a current sheet of width 2a required to excite the K-H instability for $k_\parallel = 0$. Since nonzero values of $k_\parallel$ tend to stabilize the instability larger ΔV will be required to excite the instability in those cases where $k_\parallel > 0$ [*Peñano and Ganguli*, 2000]. For the purpose of estimating the maximum unstable width for small-scale current sheets ($a < [\Sigma_P/K]^{1/2}$) however we take $k_\parallel = 0$ and assume that $J_\parallel = K\phi_{\mathrm{msphere}}$ where K is the field line conductance and ϕ_{msphere} is the electrostatic potential across the current sheet at altitudes above the region of parallel electric field [*Lysak*, 1990] in the magnetosphere. Taking $V_{1Y} = E_{X\ \mathrm{msphere}}/B_{o\ \mathrm{msphere}} = \phi_{X\ \mathrm{msphere}}/(B_{o\ \mathrm{msphere}}a)$) and substituting the current voltage relation into 1 we find that the range of auroral arc widths unstable to the K-H instability is given by

$$a^2_{msphere} < \frac{1}{B_{o\ msphere}K} \sqrt{\frac{\rho_{msphere}}{\mu_o}} \qquad (2)$$

This result demonstrates the growth of the K-H instability requires finite field-line conductance and that more resistive field-lines will be more unstable to this instability. Taking typical parameters above the topside ionosphere ($n \approx 1\ \mathrm{cm}^{-3}$; *Strangeway et al.* [1998]; $B_o = 10^{-5}\ \mathrm{nT}$) and K = 1 × 10^{-9} (ohm m^2)$^{-1}$ [*Lyons*, 1981] we find that current sheets with half-widths less than ~2km can be unstable to the K-H instability.

[5] Significantly this width is similar to the electron inertial length above the topside ionosphere. At this scale slippage between the geomagnetic field and the plasma becomes significant and auroral current sheets become unstable to the tearing instability [*Seyler*, 1990]. Consequently, for typically observed parameters on auroral field lines the K-H and tearing instabilities can be expected to operate on auroral arcs of similar widths. The growth rate of the tearing instability varies inversely with the transverse Alfvén transit time across the sheet [*Furth et al.*, 1963] so that current sheets are increasingly unstable to this instability as they become narrower and as $J_\parallel$ is increased. However, sheared flows, which generally increase with decreasing current sheet width, tend to stabilize the tearing instability [*Chen et al.*, 1997] when the time for the flow to traverse one wavelength along the current sheet is less than the Alfven transit time across the current sheet. For the same current sheet geometry discussed above, this means that for wavelengths

of the order of 2a, tearing will be preferred under conditions where $|E_X/B_Y| < V_A$. Consequently, a key factor in determining the evolution of auroral current sheets is the relationship between ΔV and $J_\parallel$, or in terms of easily measured electric and magnetic field quantities, the relationship between the change of the electric field (ΔE_X) and magnetic field (ΔB_Y) across the current sheet.

[6] In this report we extend this qualitative discussion to include the physics of inertial Alfven waves and examine through simulations the evolution of current sheets on kilometer scales such as those embedded within the onset arc identified by *Mende et al.* [2003]. We show how these sheets evolve to form commonly observed auroral features and discuss the instabilities and dynamics active in their formation. In performing these simulations our selection of plasma parameters and current sheet equilibria are in part guided by observations from the FAST spacecraft associated with Mende's and similar events. We note that this work differs from that considered by *Seyler* [1990] and *Wu and Seyler* [2003] through the use of a plasma model derived from observations where the Kelvin-Helmholtz instability in addition to the tearing instability is active. It is largely the interplay between these instabilities, the effective field-line conductance and reflection from the topside ionosphere that determine the current sheet evolution. This interaction provides new insights into the evolution of auroral forms not present in previous studies that are particularly relevant to recent observations which identify distinct discrete auroral acceleration mechanisms known as the "Alfvénic" and "Quasi-static" or "Inverted-V aurora." We note that while this work is motivated by Mende's observations, it is also relevant to poleward boundary intensifications [*Lyons et al.*, 1999] and generally to the evolution of small-scale auroral forms.

2. Simulation Approach

[7] We use a reduced-MHD model for an incompressible plasma where the evolution of the scalar (ϕ) and vector ($A_\parallel$) potentials are governed by the vorticity and induction equations given by

$$B_o \frac{\partial \nabla_\perp^2 \phi}{\partial t} + \hat{z} \times \nabla_\perp \phi \bullet \nabla_\perp \nabla_\perp^2 \phi - V_A^2$$
$$\cdot \left(B_o \frac{\partial \nabla_\perp^2 A_\parallel}{\partial z} + \hat{z} \times \nabla_\perp A_\parallel \bullet \nabla_\perp \nabla_\perp^2 A_\parallel \right) = 0 \qquad (3)$$

$$\frac{\partial}{\partial t} \left(A_\parallel - \lambda_e^2 \nabla_\perp^2 A_\parallel \right) + \hat{z} \times \nabla_\perp \phi \bullet \nabla_\perp \left(A_\parallel - \lambda_e^2 \nabla_\perp^2 A_\parallel \right)/B_o - \frac{\partial \phi}{\partial z}$$
$$- \frac{1}{\mu_o} \eta(z) \nabla_\perp^2 A_\parallel = 0, \qquad (4)$$

respectively, where λ_e is the electron inertial length. Because similar models have been used previously to study the evolution of auroral current sheets we present these equations here without derivation and refer to the work of *Seyler* [1990] and others where their derivation and properties are described in detail [*Shukla and Stenflo*, 1999; *Streltsov et al.*, 1990; *Chmyrev et al.*, 1992]. We will discuss the important differences in our implementation momentarily but first describe some of the assumptions on which this model is based. Primarily, the validity of this model above the aurora is predicated on the strong geomagnetic field that exists

there. For strong B_o structuring in the perpendicular direction is energetically preferable to that in the parallel direction and consequently we consider length scales $L_\perp/L_\parallel \ll 1$. Under these conditions the plasma can be considered incompressible so that magneto-sonic waves are not included in the model (hence the term "reduced" and the consideration of $A_\parallel$ and ϕ alone) and Fourier analysis of equations (3) and (4) yields the dispersion relation for inertial Alfvén waves [*Lysak and Carlson*, 1981]. It should also be noted that being an MHD model equations (3) and (4) do not include the physics of waves with frequencies approaching the ion gyrofrequency nor does it include that of double layers but does allow for resistive layers which may serve as a proxy for the microphysics inaccessible to our fluid approach [*Lysak and Hudson*, 1987]. In addition to differences in the plasma model and initial equilibria used, our implementation differs from that performed previously in auroral studies through the inclusion of resistivity (η) along the magnetic field. This appears in the last term of equation (4) and is included to provide finite K along our model field-lines similar to that observed through quasi-static aurora as described in the introduction. For the purposes of this work we do not associated $\eta(Z)$ with any specific microphysics but rather define its profile along B_o from observations.

[8] Equations (3) and (4) are solved using a leapfrog scheme in a domain representing a portion of the geomagnetic field extending from the conducting ionosphere at 100 km up to 10,200 km in altitude (Z-64 pts) and 20 km and 10 km in the east-west direction (Y-256 pts) and north-south (X-128 pts) directions, respectively. We have performed runs with larger dimensions in Z (and also X and Y) but the pertinent results remain unchanged. The density profile includes magnetospheric and ionospheric components taken to be H_+ with $n_H^+ = 3$ cm^{-3} and O^+ with $n_{O+} = 10^{4.1}e^{(-h/300)}$ cm^{-3}, respectively where h is the altitude in kilometers. λ_e above the topside ionosphere is 3100 m. The geomagnetic field is assumed to be vertical and uniform with a value of $B_o = 1.3 \times 10^{-5}$ T which is the approximate strength of the geomagnetic field at 4000 km altitude. The use of a uniform field means scale sizes are referenced to this altitude (unless indicated otherwise). Based on a dipole field the transverse spatial scaling factor between 4000 km and the upper and ionospheric boundaries is ~4 and ~2, respectively. This density profile and magnetic field provides an Alfvén speed profile constant in altitude above 3500 km but decreasing toward the ionosphere in a manner analogous to that inferred from polar orbiting spacecraft.

[9] We use a spectral technique based on 2-D Fourier transforms for the solution of the nonlinear terms in the plane perpendicular to the geomagnetic field. Aliasing is avoided by filtering in k-space using the function $\exp[-(k_x/k_{x\_max})^n - (-k_y/k_{y\_max})^n]$ with n = 8. This function attenuates variations at the largest wave numbers (smallest scales) while leaving variations at the wave numbers of most interest unaltered. We have implemented other antialiasing techniques and find little difference in results at the cost of longer computation time. A Heun technique is used for the time advance and provides a stable solution over the duration of each run. The Courant condition is satisfied by a factor of 2 throughout. The boundary condition at the ionospheric end follows from current continuity and is given by $A_\parallel + \mu_o\phi\Sigma_p = 0$ for uniform Σ_P which we take to be 1 mho.

At the magnetospheric end we use an open boundary condition defined by *Lysak* [1985] and given by the effective impedance of inertial Alfvén waves as $A_\parallel + \mu_o\phi\Sigma_A = A_o(t)$ where $\Sigma_A = [\mu_o V_A \sqrt{1 + k_\perp^2 \lambda_\theta^2}]^{-1}$. The boundary conditions in the transverse directions are periodic. To provide a $J_\parallel$ profile similar to a section of that observed in the onset arc of *Mende et al.* [2003] we use $J_o(x,t) = C(t)[\cosh^{-2}(\kappa 2\pi x) - \tanh(\kappa\pi)/(\kappa\pi)]$ where $-1 \leq x \leq 1$ over the width of the simulation domain in the north-south direction and C(t) is function representing the applied $J_\parallel$ amplitude at the magnetospheric end of the simulation. C(t) increases from zero to 7.5 $\mu A/m^2$ over a small fraction of the simulation time. The applied $J_\parallel$ is uniform in the east-west direction (Y) and for $\kappa = 2$ consists of a central upward current with width in the north-south direction of 3/4 λ_e or 2.3 km bracketed by two broader downward currents. The current is perturbed in the y direction by the application of a k_y^{-2} noise spectrum composed of sine waves with random phases. The amplitude of the perturbation is ≤ 0.01 $\mu A/m^2$. We note that we have tried alternative functional forms for J_o and find similar results provided the relative width of the upward and downward sheets is similar.

[10] The form of $\eta(Z)$ follows from the Vlasov solutions by *Ergun et al.* [2000] for observed particle distributions through the "quasi-static" or "inverted-V" aurora. These indicate an asymmetric profile in E_Z at the interface between the magnetospheric and ionospheric plasma dominated sections of the flux tube. To mimic such a feature in our fluid model, and thereby the "quasi-static" aurora, we impose a resistive layer with the profile $\eta(Z) = \eta_o e^{1 - \frac{|z-z_\eta|}{h_\eta} - \exp\left[-\frac{|z-z_\eta|}{h_\eta}\right]}$ where Z_η is the altitude of peak resistivity chosen to be 3500 km and $h_\eta = 50$ km and $h_\eta = 200$ km below and above Z_η, respectively. We note that this layer may be composed of one or more double layers [*Ergun et al.*, 2004]. For consistency with current-voltage studies of the aurora as used in the derivation of equation (2), we take $\eta_o = 2000$ ohm m which provides a field line conductivity of K = 1×10^{-9} $(ohm$ $m^2)^{-1}$ as derived from observations through inverted-V arcs [*Lyons*, 1981].

[11] To aid in understanding the simulation results we now consider the expected time-scales for the evolution of the system. For the plasma model described above the Alfven transit time from the magnetospheric boundary to the topside ionosphere is 0.04 s (without inertial correction) and to the ionospheric boundary is 0.85 s. The approximate Alfven transit time based on the imposed transverse magnetic field (a few nT) of the current sheet across the central upward current sheet is ~0.05 s. This is also the approximate expected growth timescale or e-folding time of the tearing instability at $k_y\lambda_e \sim 1$ [*Seyler*, 1990]. The magnetospheric boundary condition for the magnetic field and scale of the current sheet provides a transverse electric field (≤ 1 V/m) so that the approximate expected minimum growth time scale of the Kelvin Helmholtz instability $((\Delta V/2a)^{-1})$ [*Biskamp*, 2003] is of the order of 0.03 s. We note that these time scales are significantly less than the Alfven transit time from the source region in the equatorial plane of the magnetosphere or the growth time scale for plasma sheet instabilities which drive the evolution of larger-scale auroral morphology [*Angelopoulos et al.*, 2008]. Consequently the small-scale structuring will be defined by the action of local instabilities, as we study here, rather than processes active closer to the current source regions.
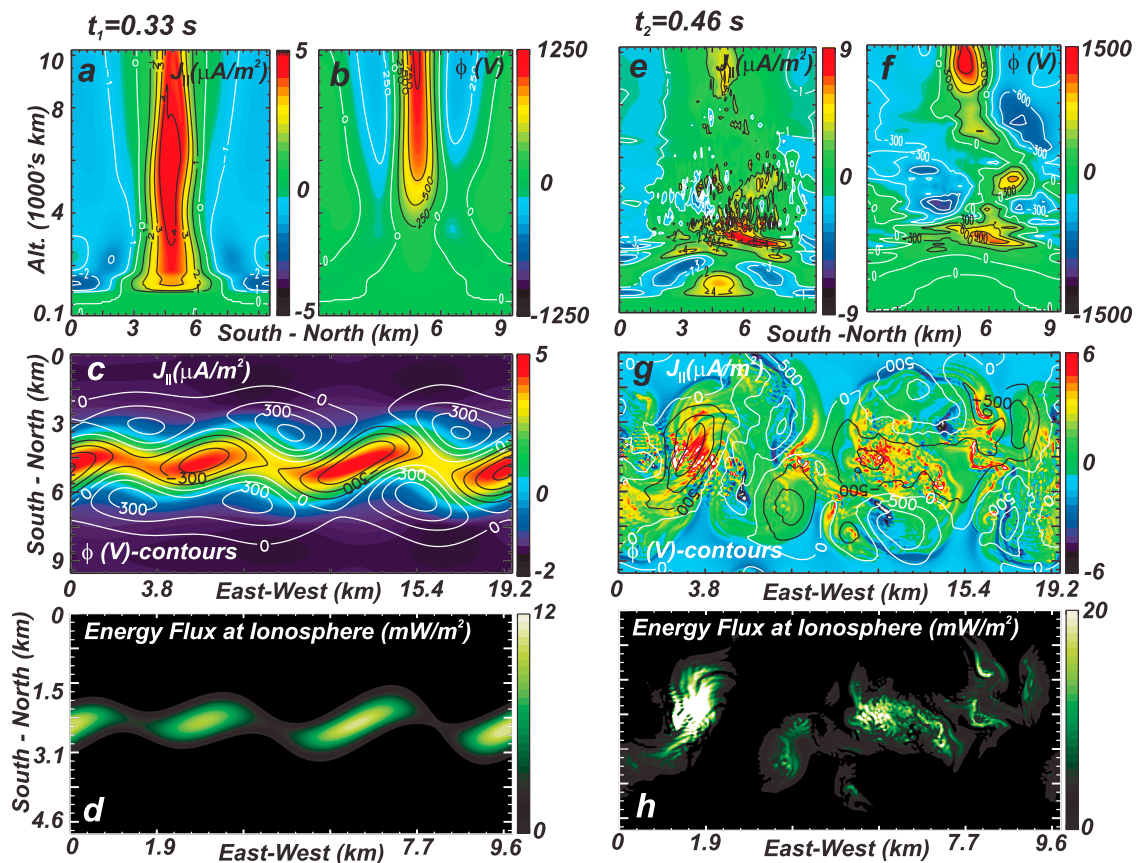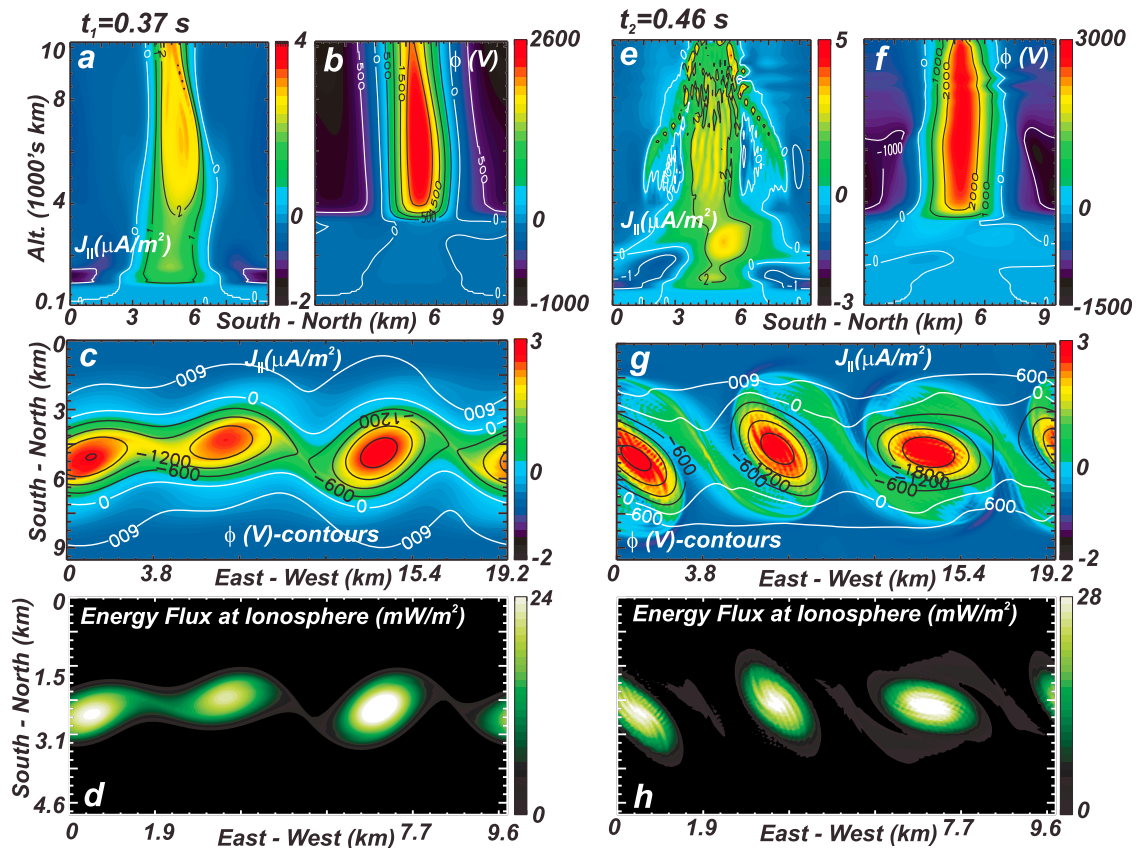
Figure 1. Current sheet evolution snapshots from the run without a resistive layer. (a and b) Vertical slices in the South-North (X) direction through the simulation domain taken 500 m from the eastern boundary or left-hand edge shown in Figure 1c; Figures 1a and 1b show $J_\parallel$ and ϕ, respectively. (c) A transverse slice through the simulation domain at 4500 km altitude; the color scale shows $J_\parallel$ and the contours show ϕ. B_o is out of the page. (d) The downgoing energy flux at 100 km altitude scaled with the geomagnetic field. (e–h) The same as Figures 1a–1d but at the later time.

[12] Inclusion of resistivity in the simulation introduces a diffusive time scale (τ_{rd}) which for the profile we defined above is sharply peaked at 3500 km altitude. At this altitude $\tau_{rd} = \mu_o(2a)^2/\eta_o = 0.0033$ s and remains less than the growth time scale of the K-H instability over a range of ~400 km centered on this peak. Consequently diffusion will act to broaden or smooth out the current over this narrow range more rapidly than the instabilities mentioned above drive structuring. This broadening may eventually stabilize the instability over this altitude range. The effects of this are apparent in the simulation results, however, we note that the energetic electrons, which carry current and produce aurora, will pass rapidly through this altitude range and may be expected to faithfully represent the structure of the current sheet above the resistive layer [*Hallinan*, 1981] as they precipitate into the ionosphere.

3. Simulation Results

[13] We consider two scenarios: one where the resistivity is zero everywhere and electron inertia acts alone leading to a highly structured potential profile perhaps consistent with the "Alfvénic aurora" (Figure 1), and a second including the resistive layer defined above, leading to a "quasi-static/inverted-V" like potential structure (Figure 2). Initially the evolution observed in each scenario is identical and begins with the time variation of $J_o(t)$ at the magnetospheric boundary giving rise to polarization currents which close-upward and downward $J_\parallel$. This launches an inertial Alfvén wave which propagates down the geomagnetic field. The upward and downward $J_\parallel$ sheets following the wavefront form field-aligned layers of excess negative and positive charge, respectively. The associated converging and diverging electrostatic fields drive oppositely directed ExB_o/B_o^2 flows on either side of the charge layers so that a velocity shear exists across each current sheet. Due to electron inertia, ΔV across the upward $J_\parallel$ sheet exceeds $2V_{A\perp}$, or equivalently $\Delta E_X/\Delta B_Y > V_A$, and we find based on the configuration of the vortices formed (as we will discuss momentarily) that the current sheet is K-H unstable. The K-H instability therefore drives the growth of vortices behind the wavefront as it propagates downward and dominates the evolution of the current sheets before the wavefront reaches topside ionosphere. After this time the evolution for the cases with and without the resistive layer diverge.

Figure 2. Current sheet evolution snapshots from the run with a resistive layer. (a and b) Vertical slices in the South-North (X) direction through the simulation domain taken 500 m from the eastern boundary or left-hand edge shown in Figure 2c; Figures 2a and 2b show $J_{\parallel}$ and ϕ, respectively. (c) A transverse slice through the simulation domain at 4500 km altitude; the color scale shows $J_{\parallel}$ and the contours show ϕ. B_o is out of the page. (d) The downgoing energy flux at 100 km altitude scaled with the geomagnetic field. (e–h) The same as Figures 2a–2d but at the later time.

[14] Figures 1a and 1b show a vertical north-south slice through the simulation at time $t_1 = 0.33$s for the case with the no resistive layer. By this stage the leading edge of the current shown in Figure 1a has reached the topside ionosphere at 3500 km. The field-aligned gradients in potential shown in Figure 1b comprise the electrostatic portion of a parallel electric field supported by electron inertia and given by the parallel component of the electron momentum equation as $E_{\parallel} = \lambda_e^2(\partial J_{\parallel}/\partial t - \mathbf{z} \times E_{\perp}/B_o \cdot \nabla J_{\parallel})$ where $\hat{z}$ along B_o. The field-aligned potential drop through the central upward current sheet at this time is ~1 kV - this is however somewhat transitory as the presence of the parallel field at this stage is partly dependent on temporal variations in the current and reflection from the ionosphere can lead to partial cancellation. At this time much of the downgoing Poynting flux in fact is being reflected from the steep Alfvén speed gradient just below this altitude. Because of the positive gradient in $\Sigma_A = 1/\mu_o V_A$ here, $E_{\perp}$ in the reflected wavefront is reversed and partially cancels the electric field established by the incoming wavefront in a manner previously discussed by *Lysak and Dum* [1983]. The reflection process in this case progressively reduces ΔV ($\Delta E_{\perp}$) as the Alfvén wavefront propagates back up the field-line, thereby stabilizing the K-H instability, while simultaneously enhancing $J_{\parallel}$ ($\Delta B_{\perp}$).

[15] Figure 1c shows a transverse cross-section of $J_{\parallel}$ at 4500 km altitude with B_o out of the page. The initially planar current sheet now contains an array of semiperiodic distortions and enhancements primarily as a consequence of the K-H instability. This interpretation is supported by the potential contours, shown in black, which are centered on the $J_{\parallel}$ enhancements and indicate counter clockwise rotating flows around B_o consistent with the initial large-scale flow shear across the sheet. However, in addition, Figure 1c reveals clockwise rotating vortices, shown by the white contours, that constitute eddies in the larger-scale flow shear across the sheet. The resulting pattern of counter rotating vortices has a quadrupolar structure canted relative to the main axis of the current sheet in the same sense as the sheared flow across the sheet and centered on the thinnest portions of the sheet. This pattern is characteristic of the operation of the tearing instability [*Seyler*, 1990] in the presence of a sheared flow. This instability begins to dominate the evolution as the flow shear is reduced through wave reflection as mentioned above. In this case, reconnection of the current sheet's magnetic field is facilitated by electron inertia [*Seyler*, 1990]

and acts to stretch the vortices initially formed by the K-H instability. To provide an indication of the aurora associated with this structure Figure 1d shows the energy flux derived from $J_\parallel$ shown in 1c multiplied by the potential difference along the geomagnetic field between this altitude and the ionosphere. This is the energy flux of electrons which carry the wave current in the magnetospheric portion of the flux tube and pass through the field-aligned potential drop above the topside ionosphere to form aurora. For the sake of comparison with observations we have mapped the scales and energy fluxes to the geomagnetic field strength at 100 km altitude. The results show a series of small-scale folds or ripples similar to those found in narrow field camera observations of the aurora [*Hallinan and Davis*, 1970; *Trondsen and Cogger*, 1998]. At subsequent times these forms steepen in a counter-clockwise sense to provide a series of parallel bands.

[16] Figures 1e–1f show that this smooth structure ultimately breaks up. At $t_2 = 0.46$s the large-scale regions of upward and downward $J_\parallel$ still exist, however, they are dominated by smaller scale more intense features. The structuring is found to proceed in both the transverse and parallel directions suggestive of the operation of a third instability which unlike the K-H and tearing instabilities grows most strongly for finite $k_\parallel$. Inspection of Figure 1g reveals both filamentary and distorted sheet like features along the geomagnetic field at this time with structuring that eventually extends to the grid scale. While not apparent from these snapshots, the structuring appears first at those locations with the largest transverse gradients in $J_\parallel$ suggesting that the responsible instability is that identified by *Wu and Seyler* [2003] as a "current convective interchange" instability. The potential contours associated with these fine-scale currents, as shown in Figure 1g, indicate a disordered and highly structured flow pattern with counter-clockwise vortices (black contours) generally, though not exclusively, colocated with regions of upward current. Mapping the energy flux associated with these features to the ionosphere as shown in Figure 1h provides fine structured auroral forms which rotate in a counter-clockwise sense around B_o. These features may be consistent with what have been termed "RUFFS" in recent high-resolution camera measurements [*Dahlgren et al.*, 2010] and may account for the fine-scale features resolved by *Maggs and Davis* [1968].

[17] Figure 2 shows results for the same initial conditions but with the inclusion of the resistive layer discussed in section 2. Once the leading edge of the current sheet reaches the resistive layer the $\eta J_\parallel$ contribution to $E_\parallel$ dominates the establishment of the net field-aligned potential through the simulation domain. This is manifest as the closely spaced horizontal potential contours apparent below 4000 km in Figures 2b and 2f. The generation of $E_\parallel$ here is largely electrostatic with $|\partial\phi_\parallel/\partial z| \gg |\partial A_\parallel/\partial t|$ and the stability of the system is more closely represented by the current-voltage description used to derive equation (2) than the previous run. Since the conductivity of the layer is much less than the effective Alfven conductivity reflection of the leading edge of the current (which propagates as an inertial Alfven wave) from the layer causes a reversal of $B_\perp$. This results in a reduction of $J_\parallel$ ($\Delta B_\perp$) as the wavefront propagates back up the field-line and an enhancement of ΔV ($\Delta E_\perp$) and the growth rate of the K-H instability. A tearing instability does

not occur because of the flow along the current sheet significantly exceeds the transverse Alfven speed and thereby does not allow the formation of magnetic islands (at least on scales that can fit within the simulation). The consequences of the action of the K-H instability are manifest in Figure 2c where we find nearly circular counter clockwise rotating vortices centered on regions of enhanced $J_\parallel$.

[18] Mapping the energy flux to the ionosphere in Figure 2d we find elliptically shaped counter-clockwise rotating patches around B_o connected by narrower and less intense energy fluxes that appear to be wound onto the rotating forms. These features have the appearance of auroral curls [*Hallinan and Davis*, 1970]. However, the thin filaments usually observed adjoining adjacent vortices are broadened and diminished somewhat due to diffusion through the resistive layer in our simulation. Inspection of horizontal slices in $J_\parallel$ at altitudes well above the resistive layer (not shown) exhibit more pronounced adjoining filaments since the diffusive time scales there are much longer than the growth time scale of the instability. With this in mind a test particle approach for determining the morphology of the auroral forms from the simulation may be more appropriate. At later times Figures 2e–2h show the production of smaller-scale features as observed in the case without the resistive layer, however these features are less prominent and there is evidence in Figure 2e that the resistive layer has broaden the current sheet close to the 3500 km altitude peak in η. The cross-section of $J_\parallel$ in Figure 2g shows the same localization of current observed at $t = 0.37$s albeit more "wound up." Mapping the energy flux of these features to the ionosphere as shown in Figure 2h reveals isolated rotating elliptical patches similar to those reported from narrow field camera observations by *Trondsen and Cogger* [1998]. At times later than shown here, these features merge and elongate to reform a planar-like arc, albeit with significant internal structure, and the process of K-H vortex formation is repeated.

[19] Figures 1 and 2 demonstrate that small-scale auroral forms at the foot points of nonresistive and resistive geomagnetic field-lines evolve toward different forms. These differences are a consequence of instabilities whose action is dependent on the magnitude of the flow shear and the strength of the field-aligned current. As shown in the introduction, and mentioned in the description of Figures 1 and 2 given above, this dependency can be expressed in terms of the value of $|E_X/B_Y|$ relative to V_A and in the case of a simple current-voltage relation can be used to define a maximum unstable width (see equation (2)). We now show quantitatively how the simulation results are in general consistent with this dependency and demonstrate how the value of $|\Delta E_X/\Delta B_Y|$ across a kilometer-scale auroral current sheet regulates its evolution. Figure 3a presents the value of $|\Delta E_X/\Delta B_Y|/V_A$ averaged along the length of the upward current sheet as a function of time. These averages are performed at the same altitude as the snapshots shown in Figures 1 and 2 (4500 km). The solid trace in Figure 3a shows this ratio for the simulation run with no resistive layer (Figure 1) and the dashed trace is for the case with the resistive layer (Figure 2). The horizontal line at fixed $|\Delta E_X/\Delta B_Y|$ is the Alfven speed. The relationship between ΔE_X and ΔB_Y is initially defined by the magnetospheric boundary condition and the form of the applied current. Because of the
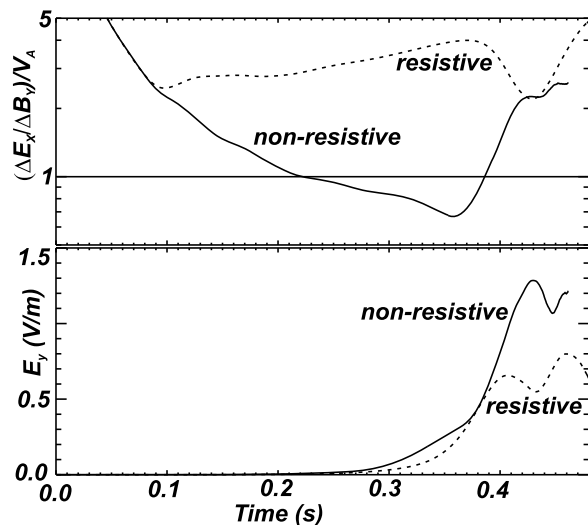
Figure 3. Time variation of average (a) $\Delta E_X/\Delta B_Y$ across the current sheet and (b) peak E_Y at 4500 km altitude. Solid lines correspond to the case without the resistive layer and dashed lines to the case with the resistive layer.

narrow width of the current this provides a value $|\Delta E_X/\Delta B_Y| > V_A$ which progressively decreases with time as the leading edge of the current sheet encounters the upper reaches of the ionosphere. The effects of wave reflection from the resistive layer become apparent after 0.09 s where the dashed and solid lines begin to diverge. Subsequently the value of $|\Delta E_X/\Delta B_Y|$ in the case without the resistive layer (solid lines) continues to decrease and at the time of the snapshots shown in Figures 1a–1d (t = 0.33 s) we find $|\Delta E_X/\Delta B_Y| < V_A$. As already described, in Figure 1c at this time the morphology in $J_{||}$ and φ is consistent with action of the tearing instability. Conversely, in the case with the resistive layer (dashed lines) and at the time of the snapshots shown in Figures 2a–2d we have $|\Delta E_X/\Delta B_Y| > V_A$. As already described, in Figure 2c at this time we find the morphology in $J_{||}$ and φ is consistent with the K-H instability. These results are consistent with the qualitative predictions given in the introduction for the suppression of the K-H instability for flows less than the Alfven speed and the suppression of the tearing instability at large flow speeds. Inspection of the morphology in $J_{||}$ and ϕ at times other than shown in Figures 1 and 2 generally adhere to this pattern except after t = 0.4 s. At these times we find that the value of $|\Delta E_X/\Delta B_Y|$ in the case without the resistive layer increases to values exceeding V_A. This is a consequence of the growth of the third instability identified above as the "current convective instability" [*Wu and Seyler*, 2003] that operates on smaller scales, grows on the steep transverse $J_{||}$ gradients, promotes large $k_{||}$ and generates large localized electric fields.

[20] The action of these instabilities in accordance with the change in $|\Delta E_X/\Delta B_Y|$ can be identified from the growth of the component of the electric field in the plane of the current sheet (E_y or east-west component). Initially this has a value of zero but grows with structuring/vortex formation along the current sheet due to the action of instabilities. Figure 3b shows the average peak amplitude of this component over a horizontal slice at 4500 km where again the solid lines and dashed lines correspond to the cases without

and with the resistive layer, respectively. The solid line is clearly not well described by a single exponential and is indicative of the operation of more than one instability. As the value of $|\Delta E_X/\Delta B_Y|$ decreases and the K-H instability is stabilized the tearing instability acts alone leading to a decrease in the growth rate of E_y after 0.3 s where we find an e-folding time similar to that estimated in the introduction for this instability. Then after 0.38 s the growth rate increases as the current convective instability drives growth at small scales leading to the increase in $|\Delta E_X/\Delta B_Y|$ mentioned above. The localized nature of $E_\perp$ generated by this instability however means the large-scale flow remains less than $V_{A\perp}$ and the tearing instability continues to be active. This evolutionary sequence has been confirmed through the inspection slices in ϕ and $A_{||}$ at this altitude which show the suppression of the K-H instability as the flow shear decreases with $|\Delta E_X/\Delta B_Y|$, the formation X-lines and magnetic islands in the plane perpendicular to B_o, and the distortion of these at small scales with onset of the current-convective instability. In contrast, with the resistive layer present, Figure 3b (dashed line) shows a single exponential form indicative of a single dominant instability up until saturation with an e-folding time of ~0.04s similar to that predicted for the K-H instability in the introduction.

4. Discussion and Conclusion

[21] These simulation results demonstrate how the instability of narrow auroral current sheets, such as those observed by *Mende et al.* [2003] at substorm onset, lead to the formation of commonly observed features in the aurora and drive the generation of small scales. These features are generally embedded within larger-scale structures and correspond to what are commonly called "arc elements" [*Hallinan and Davis*, 1970]. Our simulations indicate that the evolution of these elements is primarily due to the action of K-H and tearing instabilities followed by an instability which grows on the steep transverse gradients in $J_{||}$ generated by the former instabilities. This instability is likely that identified by *Wu and Seyler* [2003] as a "current convective interchange" instability. The dominance of the K-H or tearing instabilities is determined by the relationship between ΔV and $J_{||}$ or equivalently the value of $\Delta E_X/\Delta B_Y$ across the arc element or current sheet. Current sheets with widths of the order of kilometers above the topside ionosphere and $|\Delta E_X/\Delta B_Y|$ significantly larger than V_A will evolve predominately through the action of the K-H instability and the tearing instability will be suppressed. Conversely, if $|\Delta E_X/\Delta B_Y|$ is similar to or less than V_A then the K-H instability will be suppressed and the tearing instability will dominate. Under these low flow shear conditions the simulations show that growth rate of the current gradient instability is also larger. We note that in addition to the case study example detailed in this study we have performed simulation runs for a variety of Alfven speed and resistivity profiles along B_o and current sheet equilibria and find the same dependencies.

[22] The relationship between ΔE_X and ΔB_Y is initially defined by the "generator" which corresponds in our simulation to the magnetospheric boundary condition and the form of the applied current, but at later times is modified through reflection from the topside ionosphere. Reflection from the positive density or negative Alfvén speed gradient

here decreases $|\Delta E_X/\Delta B_Y|$ favoring the tearing and current gradient instabilities and the production of highly structured forms. Conversely, reflection off a localized resistive layer, such as a double layer, increases $|\Delta E_X/\Delta B_Y|$ favoring the K-H instability and the production of auroral curls. In this sense auroral curls may be the optical signature of double layers. These results suggest that for the same current sheet geometry, nearly electrostatic features such as those which occur in the "Quasi-static" or "inverted-V" aurora are more likely to evolve with the K-H instability. Conversely, the more electromagnetic features found in the "Alfvénic" aurora where $|\Delta E_X/\Delta B_Y| \approx V_A$ will have a more mixed evolution with the K-H, tearing and current gradient instabilities all likely to play a role.

[23] Before closing it is appropriate to acknowledge two important additional effects which may contribute to the structuring of small-scale auroral forms that are not included in our simulation model. Auroral plasmas often show steep transverse density gradients. These gradients can drive the rapid production of smaller scales and hence the structuring of auroral forms through the "phase mixing" of a larger-scale field-aligned current or Alfven wave [*Lysak and Song*, 2000]. For gradients on observed scales this process has been shown to produce many of the observed propagation characteristics of small-scale Alfvén waves above the aurora [*Lysak and Song*, 2008]. How this process is manifest in visible auroral forms is dependent on the morphology of the density distribution across the geomagnetic field but can be expected to contribute to the evolution observed. The second process involves ionospheric feedback from conductivity gradients established by electron precipitation in auroral arcs [*Lysak*, 1991]. Since the evolution we simulate occurs largely before the wavefront reflected from the conducting ionosphere returns to the acceleration region (i.e., that region above ~3000 km were finite $E_{\parallel}$ is found) we believe inclusion of an active ionospheric boundary condition would not significantly affect the results we present here. However, at latter times this effect can be expected to become important. A consideration of phase mixing and ionospheric feedback therefore remains an important task for future modeling efforts.

References

Angelopoulos et al. (2008), Tail reconnection triggering substorm onset, *Science*, *321*(5891), 931–935, doi:10.1126/science.1160495.

Biskamp, D. (2003), *Magnetohydrodynamic Turbulence*, 46 pp., Cambridge Univ. Press, Cambridge, U. K, doi:10.1017/CBO9780511535222.

Chandrasekar, S. (1961), *Hydrodynamic and Hydromagnetic Stability*, Clarendon Press, Oxford, U. K.

Chaston, C. C., C. W. Carlson, W. J. Peria, R. E. Ergun, and J. P. McFadden (1999), FAST observations of inertial Alfvén waves in the dayside aurora, *Geophys. Res. Lett.*, *26*, 647, doi:10.1029/1998GL900246.

Chen, Q., A. Otto, and L. Lee (1997), Tearing instability, Kelvin-Helmholtz instability, and magnetic reconnection, *J. Geophys. Res.*, *102*, 151, doi:10.1029/96JA03144.

Chmyrev, V. M., V. A. Marchenko, O. A. Pokhotelov, P. K. Shukla, L. Stenflo, and A. V. Streltsov (1992), The development of discrete active auroral forms, *IEEE Trans. Plasma Sci.*, *20*(6), 764, doi:10.1109/27.199525.

Dahlgren, H., A. Aikio, K. Kaila, N. Ivchenko, B. S. Lanchester, D. K. Whiter, and G. T. Marklund (2010), Simultaneous observations of small multi-scale structures in an auroral arc, *J. Atmos. Sol. Terr. Phys.*, *72*(7-8), 633–637.

Donovan, E., S. B. Mende, B. Jackel, M. Syrjäsuo, M. Meurant, I. Voronkov, H. U. Frey, V. Angelopoulos, and M. Connors (2006), The azimuthal evolution of the substorm expansive phase onset aurora, *Proceedings of International Conference on Substorms-8*, edited by M. Syrjasuo and E. Donovan, pp. 55–60, Univ. of Calgary, Calgary, Alberta, Canada.

Ergun, R. E., C. W. Carlson, J. P. McFadden, F. S. Mozer, and R. J. Strangeway (2000), Parallel electric fields in discrete arcs, *Geophys. Res. Lett.*, *27*, 4053, doi:10.1029/2000GL003819.

Ergun, R. E., L. Andersson, D. Main, Y.-J. Su, D. L. Newman, M. V. Goldman, C. W. Carlson, A. J. Hull, J. P. McFadden, and F. S. Mozer (2004), Auroral particle acceleration by strong double layers: The upward current region, *J. Geophys. Res.*, *109*, A12220, doi:10.1029/2004JA010545.

Evans, D. (1974), Precipitation electron fluxes formed by a magnetic field-aligned potential difference, *J. Geophys. Res.*, *79*, 2853, doi:10.1029/JA079i019p02853.

Furth, H. P., J. Kileen, and M. N. Rosenbluth (1963), Finite-resistivity instabilities of a sheet pinch, *Phys. Fluids*, *6*, 459, doi:10.1063/1.1706761.

Hallinan, T. J., and T. N. Davis (1970), Small-scale auroral arc distortions, *Planet. Space Sci.*, *18*, 1735, doi:10.1016/0032-0633(70)90007-3.

Hallinan, T. J. (1981), The distribution of vorticity in auroral arcs, *Physics of Auroral Formation*, Geophys. Monogr. Ser., vol. 25, edited by S.-I. Akasofu and J. R. Kan, pp. 42–49, AGU, Washington, D. C.

Lyons, L. R. (1981), The field aligned current versus electric potential relation and auroral electrodynamics, in *Physics of Auroral Arc Formation*, Geophys. Monogr. Ser., vol. 25, edited by S.-I. Akasofu and J. R. Kan, 252 pp., AGU, Washington, D. C.

Lyons, L. R., et al. (1999), Association between Geotail plasma flows and auroral poleward boundary intensifications observed by CANOPUS photometers, *J. Geophys. Res.*, *104*, 4485, doi:10.1029/1998JA900140.

Lysak, R. L. (1985), Auroral electrodynamics with current and voltage generators, *J. Geophys. Res.*, *90*, 4178, doi:10.1029/JA090iA05p04178.

Lysak, R. L. (1990), Electrodynamic coupling of the magnetosphere and the ionosphere, *Space Sci. Rev.*, *52*, 33, doi:10.1007/BF00704239.

Lysak, R. L. (1991), Feedback instability of the ionospheric resonant cavity, *J. Geophys. Res.*, *96*, 1553, doi:10.1029/90JA02154.

Lysak, R. L., and C. W. Carlson (1981), Effect of micro-turbulence on magnetosphere-ionosphere coupling, *Geophys. Res. Lett.*, *8*, 269–272, doi:10.1029/GL008i003p00269.

Lysak, R. L., and C. T. Dum (1983), Dynamics of magnetosphere-ionosphere coupling including turbulent transport, *J. Geophys. Res.*, *88*, 365, doi:10.1029/JA088iA01p00365.

Lysak, R. L., and M. K. Hudson (1987), Effect of double layers on magnetosphere-ionosphere coupling, *Laser Part. Beams*, *5*, 351, doi:10.1017/S0263034600002822.

Lysak, R. L., and Y. Song (2000), The role of Alfven waves in the formation of auroral parallel electric fields, *Magnetospheric Current Systems*, Geophys. Monogr. Ser., vol. 118, S. Ohtani et al., pp. 147–156, AGU, Washington, D. C.

Lysak, R. L., and Y. Song (2008), Propagation of kinetic Alfvén waves in the ionospheric Alfvén resonator in the presence of density cavities, *Geophys. Res. Lett.*, *35*, L20101, doi:10.1029/2008GL035728.

Maggs, J. E., and T. N. Davis (1968), Measurement of the thickness of auroral structures, *Planet. Space Sci.*, *16*, 205.

Mende, S. B., C. W. Carlson, H. U. Frey, L. M. Peticolas, and N. Østgaard (2003), FAST and IMAGE-FUV observations of a substorm onset, *J. Geophys. Res.*, *108*(A9), 1344, doi:10.1029/2002JA009787.

Otto, A., and G. T. Birk (1993), Formation of thin auroral arcs by current striation, *Geophys. Res. Lett.*, *20*, 2833, doi:10.1029/93GL02492.

Paschmann, G., S. Haaland, and R. Treumann (2003), *Auroral Plasma Physics*, Kluwer Acad. Publ., Dordrecht, Netherlands.

Peñano, J. R., and G. Ganguli (2000), Generation of ELF electromagnetic waves in the ionosphere by localized transverse DC electric fields: Subcyclotron regime, *J. Geophys. Res.*, *105*, 7441, doi:10.1029/1999JA000303.

Roux, A., et al. (1991), Plasma sheet instability related to the westward traveling surge, *J. Geophys. Res.*, *96*, 17,697–17,714, doi:10.1029/91JA01106.

Seyler, C. E. (1990), A mathematical model of the structure and evolution of small-scale discrete auroral arcs, *J. Geophys. Res.*, *95*, 17,199, doi:10.1029/JA095iA10p17199.

Shukla, P. K., and L. Stenflo (1999), Nonlinear Phenomena involving dispersive Alfven waves, in *Non-linear MHD Waves and Turbulence*, edited by T. Passot and P.-L. Sulem, 1 pp., Springer, New York, doi:10.1007/3-540-47038-7_1.

Strangeway, R. J., et al. (1998), FAST observations of VLF waves in the auroral zone: Evidence of very low plasma densities, *Geophys. Res. Lett.*, *25*, 2650, doi:10.1029/98GL00664.

Streltsov, A. V., V. M. Chmyrev, O. A. Pokhotelov, V. A. Marchenko, and L. Stenflo (1990), The formation and Nonlinear evolution of convective cells in the auroral plasma, *Phys. Scr.*, *41*, 686, doi:10.1088/0031-8949/41/5/012.

Trondsen, T. S., and L. L. Cogger (1998), A survey of small-scale spatially periodic distortions of auroral forms, *J. Geophys. Res.*, *103*, 9405, doi:10.1029/98JA00619.

Wagner, J. S., R. D. Sydora, T. Tajima, T. Hallinan, L. C. Lee, and S.-I. Akasofu (1983), Small-scale auroral arc deformations, *J. Geophys. Res.*, *88*, 8013, doi:10.1029/JA088iA10p08013.

Wu, K., and C. E. Seyler (2003), Instability of inertial Alfvén waves in transverse sheared flow, *J. Geophys. Res.*, *108*(A6), 1236, doi:10.1029/2002JA009631.

C. C. Chaston, Space Sciences Laboratory, University of California, Berkeley, CA 94720, USA. (ccc@ssl.berkeley.edu)

K. Seki, Solar Terrestrial Environment Laboratory, University of Nagoya, Nagoya, Aichi 464-8601, Japan.